Title: Host-resistance factor SLC11A1 restricts *Salmonella* growth through magnesium deprivation

Authors: Olivier Cunrath[1], Dirk Bumann[1]*

Affiliations: Biozentrum, University of Basel, CH-4056 Basel, Switzerland

*Correspondence to: dirk.bumann@unibas.ch.

Abstract: The pleiotropic host-resistance factor SLC11A1 (NRAMP1) defends against diverse intracellular pathogens in mammals by as yet unknown mechanisms. We compared *Salmonella* infection of coisogenic mice with different *SLC11A1* alleles. SLC11A1 reduced *Salmonella* replication and triggered upregulation of uptake systems for divalent metal cations but no other stress responses. SLC11A1 modestly diminished iron availability and acutely restricted *Salmonella* access to magnesium. Growth of *Salmonella* cells in presence of SLC11A1 was highly heterogeneous and inversely correlated with expression of the crucial magnesium transporter gene *mgtB*. We observed superimposable single-cell patterns in mice lacking SLC11A1 when we restricted *Salmonella* access to magnesium by impairing its uptake capabilities. Together, these findings identify deprivation of the main group metal magnesium as main resistance mechanism of SLC11A1 against *Salmonella*.

One sentence summary: A macrophage protein limits metal availability

Main text: Solute carrier family 11, member 1 (SLC11A1; also called natural resistance-associated macrophage protein 1, NRAMP1) is a host-resistance factor that controls susceptibility to the intracellular pathogens *Salmonella*, *Mycobacteria*, and *Leishmania* (*1*). SLC11A1 transports Fe^{2+}, Mn^{2+}, and Co^{2+} out of phagosomes, and may deprive vacuolar pathogens of these essential micronutrients. In addition, SLC11A1 modulates phagosome maturation; pro-inflammatory cytokines and activation of innate lymphocytes; generation of nitric oxide, reactive oxygen species, and lipocalin 2; as well as mammalian iron homeostasis (Fig. S1). The main mechanisms of SLC11A1-mediated resistance are still unclear, and metal starvation in the phagosome might be secondary to the effects of inflammatory responses and altered host iron homeostasis (*1*).

We generated coisogenic mice carrying the D169 null allele (*SLC11A1*^{s}, s) or the functional G169 allele (*SLC11A1*^{r}, r) in the C57BL/6 background. After infection with *Salmonella*, heterozygous (r/s) and particularly homozygous (r/r) mice showed delayed symptoms and reduced *Salmonella* colonization of spleen compared to (s/s) mice (Fig. 1A; Fig. S2a,b). (r/s) and (r/r) mice still succumbed to the disease from day 7 post-infection in contrast to 129S2/SvPasCrl mice which survived *Salmonella* infection indicating contributions of additional resistance loci (*2*). *SLC11A1*^{r} reduced *Salmonella* replication as measured with the growth reporter TIMER^{bac} (*3*), from 0.14 ± 0.02 h^{-1} in (s/s) mice to 0.08 ± 0.02 h^{-1} in (r/s) mice and 0.065 ± 0.01 h^{-1} in (r/r) mice, thus approximating division rates in highly resistant 129S2/SvPasCrl mice (Fig. 1B,C; Fig. S2c,d). Slow replication was maintained through day 6 post-infection, and fully explained the reduced *Salmonella* loads in (r/s) and (r/r) mice, but not in 129S2/SvPasCrl mice (Fig. 1A,C,D). SLC11A1 thus regulated *Salmonella* replication (*4*), while additional loci in 129S2/SvPasCrl mice enhanced killing of *Salmonella*.

We sorted *Salmonella* from spleen and determined their protein profiles. We analyzed (s/s) mice at day 4 as they succumbed to infection from day 5. For (r/s) and (r/r) mice, we had to wait until day 6, or use higher inocula, to obtain sufficient *Salmonella* material. SLC11A1 had similar impact on *Salmonella* growth at day 4 and 6 after infection (Fig. 1C), and after low- and high-dose infection (Fig. S1e).

Comparison of 1833 *Salmonella* proteins revealed increased abundance of uptake systems for metal cations Mg^{2+}, Zn^{2+}, $Fe^{2+/3+}$, and Mn^{2+} in (r/s) and particularly (r/r) mice (Fig. 2A, colored circles). Ribosome subunits were less abundant in (r/s) and (r/r) mice (Fig. 2A, black circles), consistent with slower *Salmonella* replication (Fig. 1C). Otherwise, *Salmonella* from the different mouse genotypes were rather similar (Fig. S3a). We did not observe signs for differential oxidative or nitrosative stress in agreement with the activities of respective *Salmonella* reporter strains (Fig. 2B; Fig. 3b) (*5*) and genetic evidence against a role of these stresses in SLC11A1-mediated resistance (*6*). Major virulence systems and metabolic and cell envelope stress regulons were also unaltered (Fig. S3a). Finally, comparison to proteomes of slow- and fast-growing *Salmonella* subsets from BALB/c (s/s) mice (*3*) (Fig. S3c) indicated fundamentally different mechanisms of *Salmonella* growth-control in presence or absence of SLC11A1. Taken together, SLC11A1 specifically induced *Salmonella* metal uptake systems but no other stress responses.

Salmonella encodes transporters with different affinities for divalent metal cations (Fig. 3A, table S1). We compared the fitness of *Salmonella* strains with single and multiple gene deletions (detailed description in Supplementary Text) in littermates from (r/s) x (s/s) crosses. We analyzed (s/s) mice after four days, and (r/s) after six days, to match the number of *Salmonella in-vivo* divisions (Fig. 3B; Fig. S4). For relevant mutants, we additionally analyzed (r/r) mice at day 4 and 6 (Fig. 3C; Fig. S4).

The quadruple iron-uptake mutant “c” had compromised fitness in (s/s) mice, a stronger defect in (r/s) mice, and almost no fitness in (r/r) mice. Available iron levels *in vivo* seemed to be generally insufficient to meet the high requirements of this mutant (30 μM iron *in vitro*, Fig. 3D), and SLC11A1 further restricted iron access (*7*). By contrast, the double iron-uptake mutant “b” retained full fitness in all three mouse genotypes indicating sufficient iron supply to meet the lower requirements of this mutant (3 μM iron *in vitro*; Fig. 3D). Wild-type *Salmonella* required even less iron and should thus not be limited by iron starvation either. SLC11A1 thus reduced iron availability but this was insufficient for limiting replication of wild-type *Salmonella*.

Mutant “e” lacking the high-affinity zinc ABC transporter had poor fitness in both (s/s) and (r/s) mice indicating limited zinc supply (*8*). By contrast, mutant “d” with a partial zinc uptake defect (*9*) had a slight, but significant fitness defects in (s/s) and (r/s) but not (r/r) mice indicating nearly sufficient access to zinc in all three mouse genotypes. Wild-type *Salmonella* with full zinc uptake capabilities would thus not be limited by zinc limitation either. Alternatively, low zinc concentration might activate host endosomal hydrolases such as cathepsins that could damage *Salmonella* cells (*10*). However, cathepsin activities did not co-localize with *Salmonella* in (s/s) and (r/s) mice (Fig. S5) (*11*). Mutants lacking uptake systems for manganese (“f”) or cobalt (“h”), or exporters for manganese (“g”) or copper (“i”) had no differential fitness defects arguing against contributions of these metals to SLC11A1-mediated resistance. Although transition metals might become more important at later disease stages with distinct host-control mechanisms (*12*) and decreasing levels of non-heme iron in spleen (*13, 14*), particularly in genetic backgrounds with lower serum iron levels (*15*), our data indicate that transition metal starvation is not required for SLC11A1-mediated resistance.

We also analyzed *Salmonella* mutants with defects in uptake systems for the main group metal magnesium, since its transporter MgtB was highly upregulated in presence of SLC11A1 (Fig. 2A). The double mutant “l” with inactivated MgtA and MgtB had severe fitness defects in all three mouse genotypes (*16*) suggesting that (i) the third magnesium transporter CorA did not contribute to magnesium uptake *in vivo* (*16*), and (ii) magnesium availability *in vivo* was insufficient to meet the requirements of this mutant. Mutant “l” might also suffer from dose-dependent iron accumulation (*17*), although this should cause the most severe fitness defects in (s/s) mice with the highest iron supply (see above), which was inconsistent with our observations. Mutant “j” with inactivated MgtA retained full fitness in all mouse genotypes (*18*), while mutant “k” with inactivated MgtB had full fitness in (s/s) mice, but compromised fitness in (r/s) and (r/r) mice (Fig. 3B,D; Fig. S3) suggesting sufficient magnesium availability only in (s/s) mice. An independently constructed Δ*mgtB* mutant had similar differential fitness phenotypes. SLC11A1 thus caused a specific requirement for MgtB (apparent K_m of 6 μM for Mg^{2+} (*19*)),

whereas MgtA with slightly lower affinity (apparent K_m 29 μM (*19*)) was dispensable in the presence of MgtB, and compensated only partially for its absence. Attenuation of *Salmonella* Δ*mgtB* in genetically resistant C3H/HeN mice (*20*), but not in susceptible BALB/c mice (*18*), has previously been reported. Our data link this phenotype to SLC11A1 instead of the many other allelic differences between C3H/HeN and BALB/c mice and suggest that SLC11A1 critically limits magnesium availability for *Salmonella*.

To determine how *mgtB* expression relates to the remarkably heterogeneous replication of *Salmonella* single-cells (Fig. 1B), we combined a *timer*^{bac} expression cassette reporting single-cell division rates (*3*), with a transcriptional fusion of the $P_{mgtCBRcigR}$ promoter driving *mgtB* expression to *bfp* (Fig. S6a-c). *Salmonella mgtB* expression and division rate were inversely correlated in (r/s) and (r/r) mice, but not in (s/s) mice (Fig. 4A,B). In presence of SLC11A1, poorly replicating *Salmonella* cells thus maximized Mg^{2+} uptake through the crucial transporter MgtB, possibly in order to compensate for magnesium limitation. To test this hypothesis, we deprived *Salmonella* of magnesium by an independent mechanism, and determined the effects in susceptible (s/s) mice that normally provide sufficient magnesium for *Salmonella* growth (see above). Consistent with our fitness data (Fig. 3B), *Salmonella mgtB* D379A had similar single-cell division rates as wild-type (Fig. 4C). Additional inactivation of MgtA abolished replication and triggered exceedingly high *mgtB* expression suggesting that *Salmonella* cells tried to maximize their Mg^{2+} uptake capabilities (Fig. 4A,C). For less severe growth restriction, we preserved functional MgtA but reduced its abundance with an inefficient ribosomal binding site or an unconventional initiation codon. While *Salmonella mgtB* D379A RBS*-*mgtA* had slightly reduced division rates, *Salmonella mgtB* D379A AUA-*mgtA* had substantially reduced division rates in (s/s) mice approximating those of wild-type *Salmonella* in (r/s) and (r/r) mice (Fig. 4A,C). By impairing magnesium uptake, we could thus achieve similar levels of growth restriction as imposed by SLC11A1. Astonishingly, this was also associated with superimposable single-cell *mgtB* expression (Fig. 4A,C). Individual *Salmonella* cells thus showed qualitatively and quantitatively equivalent responses to magnesium deprivation because of defective uptake, as to growth limitation by SLC11A1. By contrast,

123 expression of the critical zinc-transporter *znuA* poorly correlated with *Salmonella* division rate in all three
124 mouse genotypes (Fig. 4B) and showed discordant effects of limiting zinc uptake (Fig. S7a,b), consistent
125 with mutant fitness data arguing against relevant zinc deprivation (Fig. 3A,B). Together, these data
126 identify magnesium deprivation as main resistance mechanisms of SLC11A1.

127 These findings were initially surprising as SLC11A1 has been shown to transport Fe^{2+}, Mn^{2+}, and
128 Co^{2+} (*1*). However, the apparent affinities for these metals are in the low micromolar range (*21*), and it is
129 unclear how SLC11A1 should outcompete corresponding *Salmonella* transporters with 10 to 1,000 fold
130 better affinities (table S1). On the other hand, Mg^{2+} is the most abundant divalent cation in mammalian
131 cells with free concentrations around 0.5 - 1 mM in the cytosol as well as in *Salmonella*-containing
132 vacuoles early after phagocytosis (*22-24*). Bacterial cells require around 20 mM Mg^{2+} in their cytosol (*25*)
133 and proliferating *Salmonella* may quickly exhaust available Mg^{2+} in the vacuole, as leukocyte membranes
134 represent tight barriers for Mg^{2+} (*22, 23*). Indeed, Mg^{2+} transport becomes relevant for *Salmonella* growth
135 several hours after phagocytosis (*26*), but vacuolar Mg^{2+} concentration at such late time points are
136 currently inaccessible (*24*). SLC11A1 could restrict *Salmonella* access to Mg^{2+} by modulating fusion of
137 *Salmonella*-containing vacuoles with Mg^{2+}-containing vesicles (*27*), or SLC11A1 might directly transport
138 Mg^{2+} similar to some bacterial SLC11A1 orthologs (*28, 29*). Addressing these issues will require
139 overcoming challenges in purifying active SLC11A1 and establishment of Mg^{2+} transport assays without
140 unavailable radioisotope ^{28}Mg. More generally, this study demonstrates how integrated single-cell
141 analysis of pathogens can elucidate relevant mechanisms of pleiotropic host-resistance factors. This
142 strategy may be applicable to unravel mechanisms that control microbial growth in diverse environments.

143

References and Notes:

1. M. Wessling-Resnick, Nramp1 and other transporters involved in metal withholding during infection. *J Biol Chem* **290**, 18984-18990 (2015).
2. W. P. Loomis *et al.*, Temporal and anatomical host resistance to chronic *Salmonella* infection is quantitatively dictated by Nramp1 and influenced by host genetic background. *PLoS One* **9**, e111763 (2014).
3. B. Claudi *et al.*, Phenotypic variation of *Salmonella* in host tissues delays eradication by antimicrobial chemotherapy. *Cell* **158**, 722-733 (2014).
4. W. H. Benjamin, Jr., P. Hall, S. J. Roberts, D. E. Briles, The primary effect of the *Ity* locus is on the rate of growth of *Salmonella typhimurium* that are relatively protected from killing. *J Immunol.* **144**, 3143-3151 (1990).
5. N. A. Burton *et al.*, Disparate impact of oxidative host defenses determines the fate of *Salmonella* during systemic infection in mice. *Cell Host & Microbe* **15**, 72-83 (2014).
6. J. K. White, P. Mastroeni, J. F. Popoff, C. A. Evans, J. M. Blackwell, Slc11a1-mediated resistance to *Salmonella enterica* serovar Typhimurium and *Leishmania donovani* infections does not require functional inducible nitric oxide synthase or phagocyte oxidase activity. *J Leukoc Biol* **77**, 311-320 (2005).
7. M. Nairz *et al.*, Slc11a1 limits intracellular growth of *Salmonella enterica* sv. Typhimurium by promoting macrophage immune effector functions and impairing bacterial iron acquisition. *Cell Microbiol* **11**, 1365-1381 (2009).
8. S. Campoy *et al.*, Role of the high-affinity zinc uptake *znuABC* system in *Salmonella enterica* serovar Typhimurium virulence. *Infect Immun* **70**, 4721-4725 (2002).
9. P. Petrarca, S. Ammendola, P. Pasquali, A. Battistoni, The Zur-regulated ZinT protein is an auxiliary component of the high-affinity ZnuABC zinc transporter that facilitates metal recruitment during severe zinc shortage. *J Bacteriol* **192**, 1553-1564 (2010).
10. T. D. Lockwood, Lysosomal metal, redox and proton cycles influencing the CysHis cathepsin reaction. *Metallomics : integrated biometal science* **5**, 110-124 (2013).
11. K. McGourty *et al.*, *Salmonella* inhibits retrograde trafficking of mannose-6-phosphate receptors and lysosome function. *Science* **338**, 963-967 (2012).
12. P. Mastroeni *et al.*, Antimicrobial actions of the NADPH phagocyte oxidase and inducible nitric oxide synthase in experimental salmonellosis. II. Effects on microbial proliferation and host survival in vivo. *J Exp Med* **192**, 237-248 (2000).
13. D. E. Brown *et al.*, Increased ferroportin-1 expression and rapid splenic iron loss occur with anemia caused by *Salmonella enterica* Serovar Typhimurium infection in mice. *Infect Immun* **83**, 2290-2299 (2015).
14. D. E. Brown *et al.*, *Salmonella enterica* causes more severe inflammatory disease in C57/BL6 Nramp1G169 mice than Sv129S6 mice. *Vet Pathol* **50**, 867-876 (2013).
15. R. E. Fleming *et al.*, Mouse strain differences determine severity of iron accumulation in Hfe knockout model of hereditary hemochromatosis. *Proc Natl Acad Sci U S A* **98**, 2707-2711 (2001).
16. K. M. Papp-Wallace *et al.*, The CorA Mg^{2+} channel is required for the virulence of *Salmonella enterica* serovar Typhimurium. *J Bacteriol* **190**, 6517-6523 (2008).
17. S. Chamnongpol, E. A. Groisman, Mg^{2+} homeostasis and avoidance of metal toxicity. *Mol Microbiol* **44**, 561-571 (2002).
18. A. B. Blanc-Potard, E. A. Groisman, The *Salmonella selC* locus contains a pathogenicity island mediating intramacrophage survival. *EMBO J.* **16**, 5376-5385 (1997).
19. M. D. Snavely, S. A. Gravina, T. T. Cheung, C. G. Miller, M. E. Maguire, Magnesium transport in *Salmonella typhimurium*. Regulation of *mgtA* and *mgtB* expression. *J Biol Chem* **266**, 824-829 (1991).

20. E. Choi *et al.*, Elongation factor P restricts *Salmonella*'s growth by controlling translation of a Mg(2+) transporter gene during infection. *Sci Rep* **7**, 42098 (2017).
21. J. R. Forbes, P. Gros, Iron, manganese, and cobalt transport by Nramp1 (Slc11a1) and Nramp2 (Slc11a2) expressed at the plasma membrane. *Blood* **102**, 1884-1892 (2003).
22. M. E. Maguire, J. A. Cowan, Magnesium chemistry and biochemistry. *Biometals : an international journal on the role of metal ions in biology, biochemistry, and medicine* **15**, 203-210 (2002).
23. A. M. Romani, Cellular magnesium homeostasis. *Arch Biochem Biophys* **512**, 1-23 (2011).
24. N. Martin-Orozco *et al.*, Visualization of vacuolar acidification-induced transcription of genes of pathogens inside macrophages. *Mol Biol Cell* **17**, 498-510 (2006).
25. C. E. Outten, T. V. O'Halloran, Femtomolar sensitivity of metalloregulatory proteins controlling zinc homeostasis. *Science* **292**, 2488-2492 (2001).
26. R. L. Smith, M. T. Kaczmarek, L. M. Kucharski, M. E. Maguire, Magnesium transport in *Salmonella typhimurium*: regulation of *mgtA* and *mgtCB* during invasion of epithelial and macrophage cells. *Microbiology* **144**, 1835-1843 (1998).
27. P. Cuellar-Mata *et al.*, Nramp1 modifies the fusion of *Salmonella typhimurium*-containing vacuoles with cellular endomembranes in macrophages. *J Biol Chem* **277**, 2258-2265 (2002).
28. J. H. Shin *et al.*, Transport of magnesium by a bacterial Nramp-related gene. *PLoS Genet* **10**, e1004429 (2014).
29. A. T. Bozzi *et al.*, Conserved methionine dictates substrate preference in Nramp-family divalent metal transporters. *Proc Natl Acad Sci U S A* **113**, 10310-10315 (2016).
30. M. P. Hensley *et al.*, Characterization of Zn(II)-responsive ribosomal proteins YkgM and L31 in *E. coli*. *J Inorg Biochem* **111**, 164-172 (2012).
31. S. K. Hoiseth, B. A. Stocker, Aromatic-dependent Salmonella typhimurium are non-virulent and effective as live vaccines. *Nature* **291**, 238-239 (1981).
32. C. Kroger *et al.*, The transcriptional landscape and small RNAs of Salmonella enterica serovar Typhimurium. *Proc Natl Acad Sci U S A* **109**, E1277-1286 (2012).
33. C. Rollenhagen, M. Sorensen, K. Rizos, R. Hurvitz, D. Bumann, Antigen selection based on expression levels during infection facilitates vaccine development for an intracellular pathogen. *Proc Natl Acad Sci U S A* **101**, 8739-8744 (2004).
34. A. Hecht *et al.*, Measurements of translation initiation from all 64 codons in E. coli. *Nucleic Acids Res* **45**, 3615-3626 (2017).
35. C. Rollenhagen, D. Bumann, Salmonella enterica highly expressed genes are disease specific. *Infect.Immun.* **74**, 1649-1660 (2006).
36. X. J. Yu, K. McGourty, M. Liu, K. E. Unsworth, D. W. Holden, pH sensing by intracellular Salmonella induces effector translocation. *Science* **328**, 1040-1043 (2010).
37. B. Chen *et al.*, Dynamic imaging of genomic loci in living human cells by an optimized CRISPR/Cas system. *Cell* **155**, 1479-1491 (2013).
38. S. Haueter *et al.*, Genetic vasectomy-overexpression of Prm1-EGFP fusion protein in elongating spermatids causes dominant male sterility in mice. *Genesis (New York, N.Y. : 2000)* **48**, 151-160 (2010).
39. A. J. Grant *et al.*, Modelling within-host spatiotemporal dynamics of invasive bacterial disease. *PLoS Biol* **6**, e74 (2008).
40. B. Steeb *et al.*, Parallel exploitation of diverse host nutrients enhances salmonella virulence. *PLoS Pathog* **9**, e1003301 (2013).
41. R. Bruderer, O. M. Bernhardt, T. Gandhi, L. Reiter, High-precision iRT prediction in the targeted analysis of data-independent acquisition and its impact on identification and quantitation. *Proteomics* **16**, 2246-2256 (2016).
42. L. E. Edgington, M. Bogyo, In vivo imaging and biochemical characterization of protease function using fluorescent activity-based probes. *Current protocols in chemical biology* **5**, 25-44 (2013).

43. M. Miethke, M. A. J. M. M. B. R. Marahiel, Siderophore-based iron acquisition and pathogen control. **71**, 413-451 (2007).
44. L. R. Devireddy, D. O. Hart, D. H. Goetz, M. R. Green, A mammalian siderophore synthesized by an enzyme with a bacterial homolog involved in enterobactin production. *Cell* **141**, 1006-1017 (2010).
45. C. Correnti, R. K. Strong, Mammalian siderophores, siderophore-binding lipocalins, and the labile iron pool. *J Biol Chem* **287**, 13524-13531 (2012).
46. A. Ilari, F. Alaleona, P. Petrarca, A. Battistoni, E. Chiancone, The X-ray structure of the zinc transporter ZnuA from Salmonella enterica discloses a unique triad of zinc-coordinating histidines. *J Mol Biol* **409**, 630-641 (2011).
47. M. B. Moncrief, M. E. Maguire, Magnesium and the role of MgtC in growth of Salmonella typhimurium. *Infect Immun* **66**, 3802-3809 (1998).
48. E. Alix, A. B. Blanc-Potard, Peptide-assisted degradation of the Salmonella MgtC virulence factor. *Embo j* **27**, 546-557 (2008).
49. A. Sevostyanova, E. A. Groisman, An RNA motif advances transcription by preventing Rho-dependent termination. *Proc Natl Acad Sci U S A* **112**, E6835-6843 (2015).
50. G. Zhao, W. Kong, N. Weatherspoon-Griffin, J. Clark-Curtiss, Y. Shi, Mg2+ facilitates leader peptide translation to induce riboswitch-mediated transcription termination. *Embo j* **30**, 1485-1496 (2011).
51. S. V. Spinelli, L. B. Pontel, E. Garcia Vescovi, F. C. Soncini, Regulation of magnesium homeostasis in Salmonella: Mg(2+) targets the mgtA transcript for degradation by RNase E. *FEMS Microbiol Lett* **280**, 226-234 (2008).
52. E. J. Lee, E. A. Groisman, Tandem attenuators control expression of the Salmonella mgtCBR virulence operon. *Mol Microbiol* **86**, 212-224 (2012).
53. E. J. Lee, E. A. Groisman, Control of a Salmonella virulence locus by an ATP-sensing leader messenger RNA. *Nature* **486**, 271-275 (2012).
54. A. R. Gall *et al.*, Mg2+ regulates transcription of mgtA in Salmonella Typhimurium via translation of proline codons during synthesis of the MgtL peptide. *Proc Natl Acad Sci U S A* **113**, 15096-15101 (2016).
55. H. Wang *et al.*, Increasing intracellular magnesium levels with the 31-amino acid MgtS protein. *Proc Natl Acad Sci U S A* **114**, 5689-5694 (2017).
56. E. Choi, K. Y. Lee, D. Shin, The MgtR regulatory peptide negatively controls expression of the MgtA Mg2+ transporter in Salmonella enterica serovar Typhimurium. *Biochem Biophys Res Commun* **417**, 318-323 (2012).
57. E. Choi *et al.*, Elongation factor P controls translation of the mgtA gene encoding a Mg(2+) transporter during Salmonella infection. *MicrobiologyOpen*, e00680 (2018).
58. A. J. Westermann *et al.*, The Major RNA-Binding Protein ProQ Impacts Virulence Gene Expression in Salmonella enterica Serovar Typhimurium. *MBio* **10**, (2019).
59. N. Jabado *et al.*, Natural resistance to intracellular infections: natural resistance-associated macrophage protein 1 (Nramp1) functions as a pH-dependent manganese transporter at the phagosomal membrane. *J Exp Med* **192**, 1237-1248 (2000).
60. S. Buracco *et al.*, Dictyostelium Nramp1, which is structurally and functionally similar to mammalian DMT1 transporter, mediates phagosomal iron efflux. *J Cell Sci* **128**, 3304-3316 (2015).
61. M. L. Zaharik *et al.*, The Salmonella enterica serovar typhimurium divalent cation transport systems MntH and SitABCD are essential for virulence in an Nramp1G169 murine typhoid model. *Infect Immun* **72**, 5522-5525 (2004).
62. G. Fritsche, M. Nairz, S. J. Libby, F. C. Fang, G. Weiss, Slc11a1 (Nramp1) impairs growth of Salmonella enterica serovar typhimurium in macrophages via stimulation of lipocalin-2 expression. *J Leukoc Biol* **92**, 353-359 (2012).

63. D. J. Hackam *et al.*, Host resistance to intracellular infection: mutation of natural resistance-associated macrophage protein 1 (Nramp1) impairs phagosomal acidification. *J Exp Med* **188**, 351-364 (1998).
64. Y. Valdez *et al.*, Nramp1 drives an accelerated inflammatory response during Salmonella-induced colitis in mice. *Cell Microbiol* **11**, 351-362 (2009).
65. J. F. Hedges, E. Kimmel, D. T. Snyder, M. Jerome, M. A. Jutila, Solute carrier 11A1 is expressed by innate lymphocytes and augments their activation. *J Immunol* **190**, 4263-4273 (2013).
66. G. Fritsche *et al.*, Nramp1 functionality increases inducible nitric oxide synthase transcription via stimulation of IFN regulatory factor 1 expression. *J Immunol* **171**, 1994-1998 (2003).
67. C. H. Barton, S. H. Whitehead, J. M. Blackwell, Nramp transfection transfers Ity/Lsh/Bcg-related pleiotropic effects on macrophage activation: influence on oxidative burst and nitric oxide pathways. *Molecular medicine (Cambridge, Mass.)* **1**, 267-279 (1995).
68. S. Soe-Lin *et al.*, Nramp1 promotes efficient macrophage recycling of iron following erythrophagocytosis in vivo. *Proc Natl Acad Sci U S A* **106**, 5960-5965 (2009).
69. S. Soe-Lin *et al.*, Both Nramp1 and DMT1 are necessary for efficient macrophage iron recycling. *Exp Hematol* **38**, 609-617 (2010).
70. G. Fritsche *et al.*, Modulation of macrophage iron transport by Nramp1 (Slc11a1). *Immunobiology* **212**, 751-757 (2007).
71. M. Nairz, I. Theurl, F. K. Swirski, G. Weiss, "Pumping iron"-how macrophages handle iron at the systemic, microenvironmental, and cellular levels. *Pflugers Arch* **469**, 397-418 (2017).
72. S. Ammendola *et al.*, High-affinity Zn2+ uptake system ZnuABC is required for bacterial zinc homeostasis in intracellular environments and contributes to the virulence of Salmonella enterica. *Infect Immun* **75**, 5867-5876 (2007).
73. S. M. Newton, J. D. Igo, D. C. Scott, P. E. Klebba, Effect of loop deletions on the binding and transport of ferric enterobactin by FepA. *Mol Microbiol* **32**, 1153-1165 (1999).
74. K. J. F. m. l. Hantke, Ferrous iron transport mutants in Escherichia coli K12. **44**, 53-57 (1987).
75. D. G. Kehres, A. Janakiraman, J. M. Slauch, M. E. Maguire, SitABCD is the alkaline Mn(2+) transporter of Salmonella enterica serovar Typhimurium. *J Bacteriol* **184**, 3159-3166 (2002).
76. D. G. Kehres, M. L. Zaharik, B. B. Finlay, M. E. Maguire, The NRAMP proteins of Salmonella typhimurium and Escherichia coli are selective manganese transporters involved in the response to reactive oxygen. *Mol Microbiol* **36**, 1085-1100 (2000).
77. A. Ilari *et al.*, The Salmonella enterica ZinT structure, zinc affinity and interaction with the high-affinity uptake protein ZnuA provide insight into the management of periplasmic zinc. *Biochim Biophys Acta* **1840**, 535-544 (2014).
78. N. Taudte, G. Grass, Point mutations change specificity and kinetics of metal uptake by ZupT from Escherichia coli. *Biometals : an international journal on the role of metal ions in biology, biochemistry, and medicine* **23**, 643-656 (2010).
79. C. Bradbeer, P. R. Reynolds, G. M. Bauler, M. T. Fernandez, A requirement for calcium in the transport of cobalamin across the outer membrane of Escherichia coli. *J Biol Chem* **261**, 2520-2523 (1986).
80. S. P. Hmiel, M. D. Snavely, C. G. Miller, M. E. Maguire, Magnesium transport in Salmonella typhimurium: characterization of magnesium influx and cloning of a transport gene. *J Bacteriol* **168**, 1444-1450 (1986).
81. M. D. Snavely, J. B. Florer, C. G. Miller, M. E. Maguire, Magnesium transport in Salmonella typhimurium: 28Mg2+ transport by the CorA, MgtA, and MgtB systems. *J Bacteriol* **171**, 4761-4766 (1989).

Acknowledgements: We would like to thank Beatrice Claudi, Patricia Marini, Pauline Maturana, and Francesca Romana Cianfanelli for help with cloning and animal experiments, Pawel Pelczar (University of Basel Center for Transgenic Models) for help with genome editing, Stella Stevanova and Janine Bögli (Biozentrum FACS Core Facility) for sorting, Sandra Söderholm and Thomas Bock (Biozentrum Proteomics Core Facility) for help with proteomics, and Sarah Thomforde for correcting grammatical errors; **Funding**: This research was supported by Swiss National Science Foundation (Projects 310030_156818, 310030_182315) to DB; **Author contributions:** Outlined the study: DB, OC, Performed experiments: OC, Analysed data: OC, DB, Interpreted data: OC, DB, Wrote manuscript: DB with major contribution of OC; **Competing interests**: Authors declare no competing interests; **Data and materials availability**: All data is available in the manuscript or the supplementary materials. Correspondence and requests for materials should be addressed to D.B.

Supplementary Materials:

Materials and Methods

Supplementary Text

Figs. S1-S7

Table S1

References (31-81)

Figure legends

Fig. 1. SLC11A1 restricts *Salmonella* proliferation in mouse spleen

(A) Growth of *Salmonella* in spleen of *SLC11A1*$^{s/s}$ (s/s), *SLC11A1*$^{r/s}$ (r/s), *SLC11A1*$^{r/r}$ (r/r), or 129S2/SvPasCrl mice (129, data already reported in (*3*)). Each symbol represents a single mouse (****, $P< 0.0001$; One-way ANOVA of log-transformed values with Holm-Šídák correction for multiple comparisons).

(B) *Salmonella in-vivo* division rates as calculated from TIMER^{bac} data shown in Fig. S2D.

(C) Median *Salmonella* division rates in different mouse genotypes. Each symbol represents a single mouse (****, $P< 0.0001$; One-way ANOVA of log-transformed values with Holm-Šídák correction).

(D) Comparison of *Salmonella* net growth based on spleen loads shown in A, and *Salmonella* division rates (div. rates) shown in C.

Fig. 2. SLC11A1 triggers *Salmonella* metal uptake

(A) Proteome comparisons of *Salmonella* sorted from spleen with different *SLC11A1* genotypes ((s/s), day 4 after low-dose infection; (r/s), day 6 after low-dose infection; (r/r), day 4 after high-dose infection). Each circle represents a protein. Metal uptake systems are shown in color. RpmE2 increases cytosolic zinc concentration by replacing the zinc-binding ribosomal subunit L31 (*30*). Ribosomal proteins (RBS) are shown in black.

(B) Fluorescence of *Salmonella* reporter strains for reactive oxygen species (ROS) or reactive nitrogen species (RNS) (grey areas, autofluorescence; dashed lines, threshold for defining "GFP^{hi}" subsets; MFI, median GFP fluorescence intensities of "GFP^{hi}" subsets). Each circle represents a single mouse. More *Salmonella* cells had high P_{hmpA}-activity at day 6 in (r/s)

mice consistent with increasing nitric oxide exposure during disease progression (*5*) (*P*-value for One-way ANOVA with test for linear trend). *In-vitro* induction data for both promoters are shown in Fig. S3b.

Fig. 3. SLC11A1 causes a specific requirement for the *Salmonella* magnesium transporter MgtB

(A) Apparent affinities of *Salmonella* uptake systems for various metals (see table S1 for numerical values; TBDT, TonB-dependent transporters). The CbiMNQ system transports Co^{2+} but affinities have not yet been reported.

(B) Fitness of *Salmonella* mutants relative to wild-type in mice with different *SLC11A1* genotypes. Data points in the orange area indicate stronger fitness defects in presence of SLC11A1 (dashed ellipses). Averages and standard deviations for three to five mice are shown (****, $P< 0.0001$; **, $P< 0.01$; *, $P< 0.05$; two-tailed t-test with Holm-Šídák correction). Mutant "l" is shown in grey to indicate that some data points were below the limit of detection. Corresponding competitive indices (CI) are shown in Fig. S4.

(C) Fitness of selected *Salmonella* mutants. Each symbol represents an individual mouse. Statistical significance of differences to fitness in (s/s) mice was tested using One-way ANOVA with Holm-Šídák correction (****, $P< 0.0001$; ***, $P< 0.001$; **, $P< 0.01$; *, $P< 0.05$).

(D) Growth of wild-type and mutant *Salmonella in vitro*. Minimal medium was supplemented with 1 µM $FeSO_4$ and variable amounts of 2,2'-bipyridyl (left side), or variable amounts of $FeSO_4$ and no 2,2'-bipyridyl (right side). Individual data and means of two biological replicates are shown. Coarse estimates for *in-vivo* iron availabilities are shown below.

Fig. 4. Equivalent *Salmonella* single-cell responses to SLC11A1 and magnesium deprivation

(A) Single-cell density maps of *Salmonella* division rates and $P_{mgtCBRcigR}$ activities (pooled data from three to four mice). The dashed lines represent a fit to median values of (r/s) and (r/r) mice as shown in C. The dotted vertical lines show the median *Salmonella* division rate in (s/s) mice.

(B) Squared values ("goodness-of-fit") for Spearman's rank correlation between single-cell *Salmonella* division rates and promoter activities. Each symbol represents a single mouse (****, $P< 0.0001$; ***, $P< 0.001$; statistical significance of difference to values for (s/s) mice based on One-way ANOVA with Holm-Šídák correction).

(C) Median division rates and $P_{mgtCBRcigR}$ activities for *Salmonella* and mouse genotypes shown in A. Each symbol represents a single mouse. The black line represents a linear regression of data for (r/s) and (r/r) mice with 90% confidence bands shown as dashed lines. The inset is an enlargement of the most informative data range.

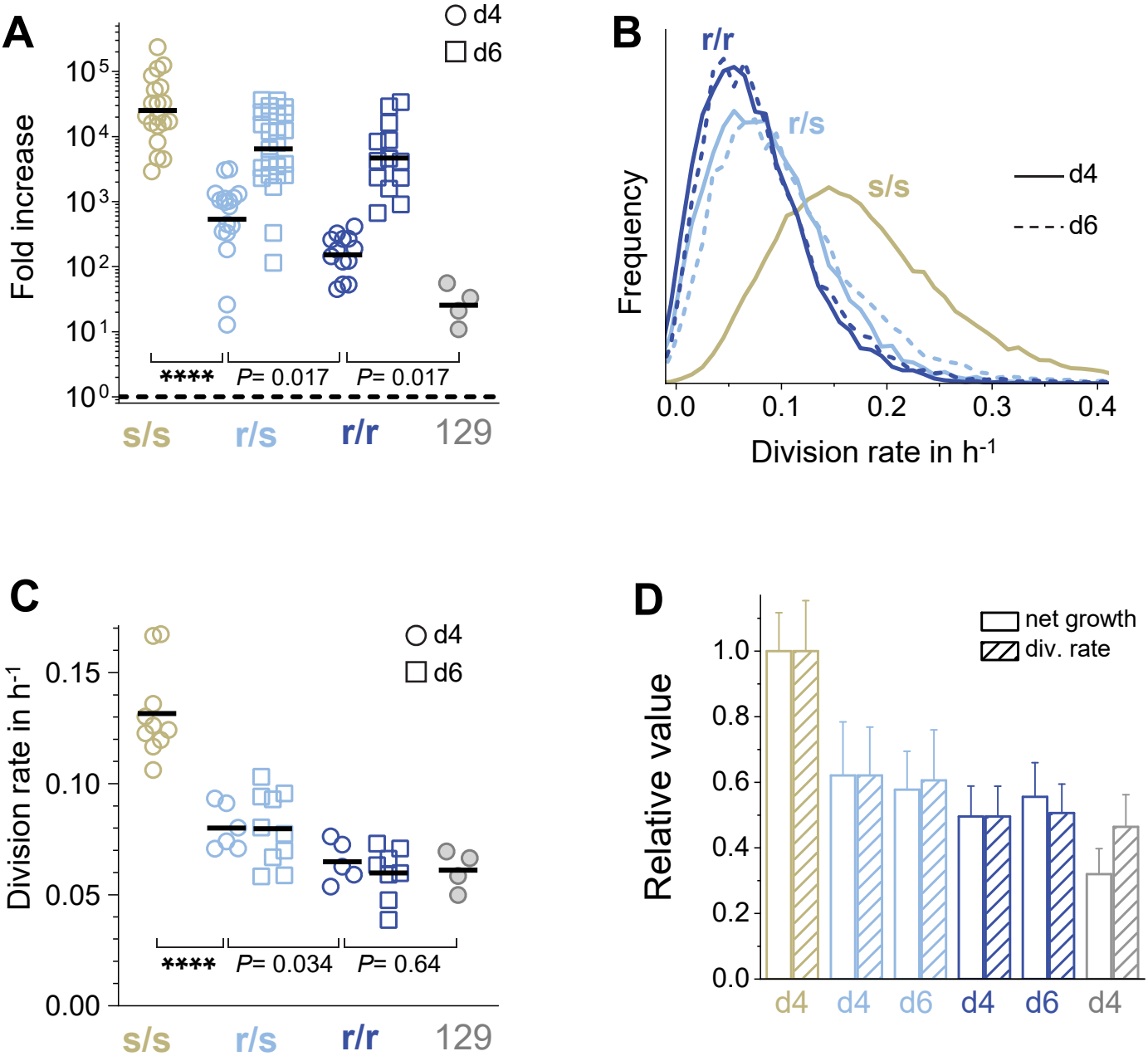
A
d4
d6
Fold increase
10^5
10^4
10^3
10^2
10^1
10^0
****
P= 0.017
P= 0.017
s/s
r/s
r/r
129
B
r/r
r/s
s/s
d4
d6
Frequency
0.0
0.1
0.2
0.3
0.4
Division rate in h^{-1}
C
d4
d6
Division rate in h^{-1}
0.15
0.10
0.05
0.00
****
P= 0.034
P= 0.64
s/s
r/s
r/r
129
D
net growth
div. rate
Relative value
1.0
0.8
0.6
0.4
0.2
0.0
d4
d4
d6
d4
d6
d4

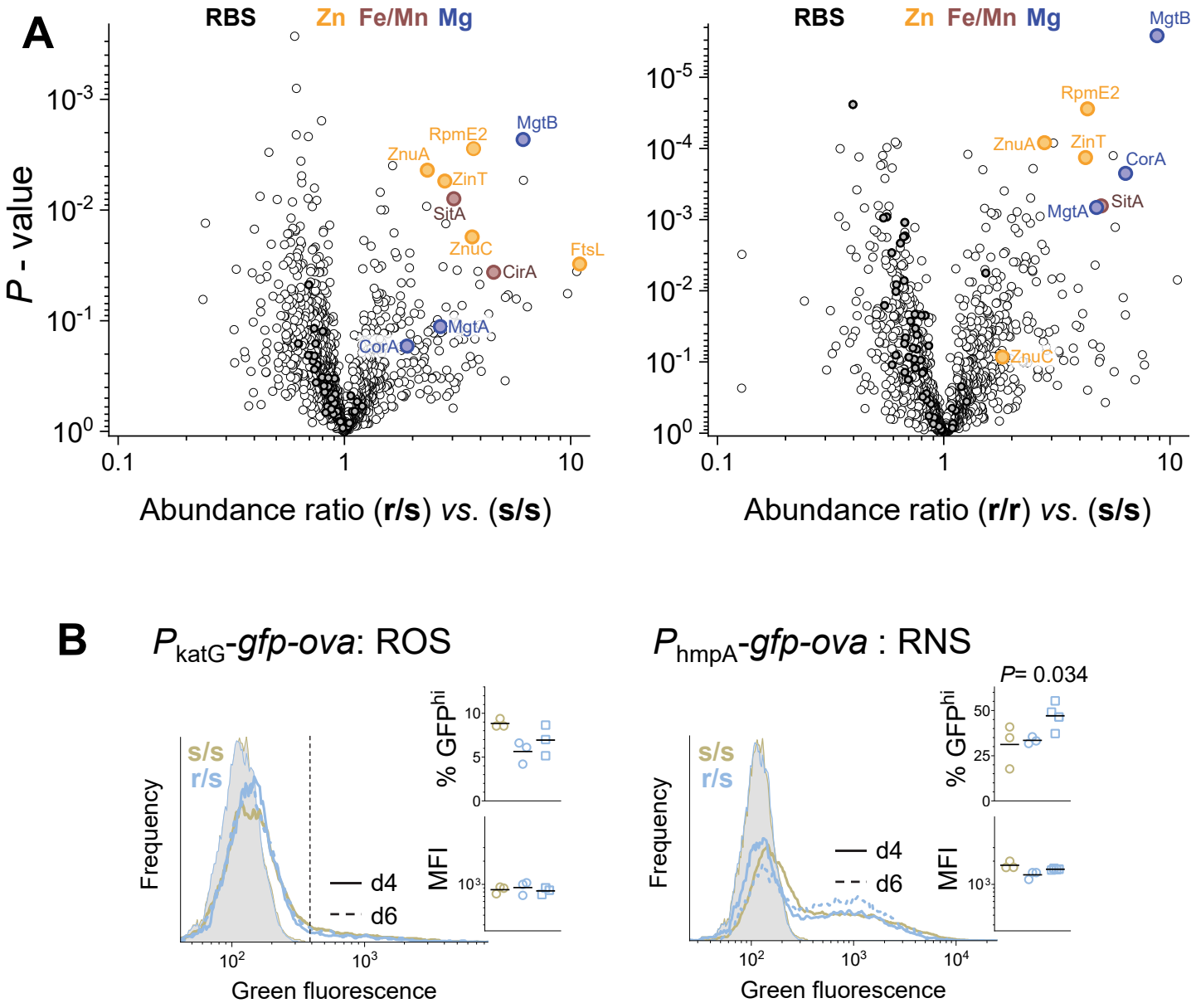
A
RBS
Zn
Fe/Mn
Mg
P - value
MgtB
RpmE2
ZnuA
ZinT
SitA
ZnuC
FtsL
CirA
MgtA
CorA
Abundance ratio (r/s) vs. (s/s)
Abundance ratio (r/r) vs. (s/s)
SitA
ZinT
CorA
B
P katG-gfp-ova: ROS
P hmpA-gfp-ova : RNS
P= 0.034
s/s
r/s
Frequency
d4
d6
% GFP hi
MFI
Green fluorescence

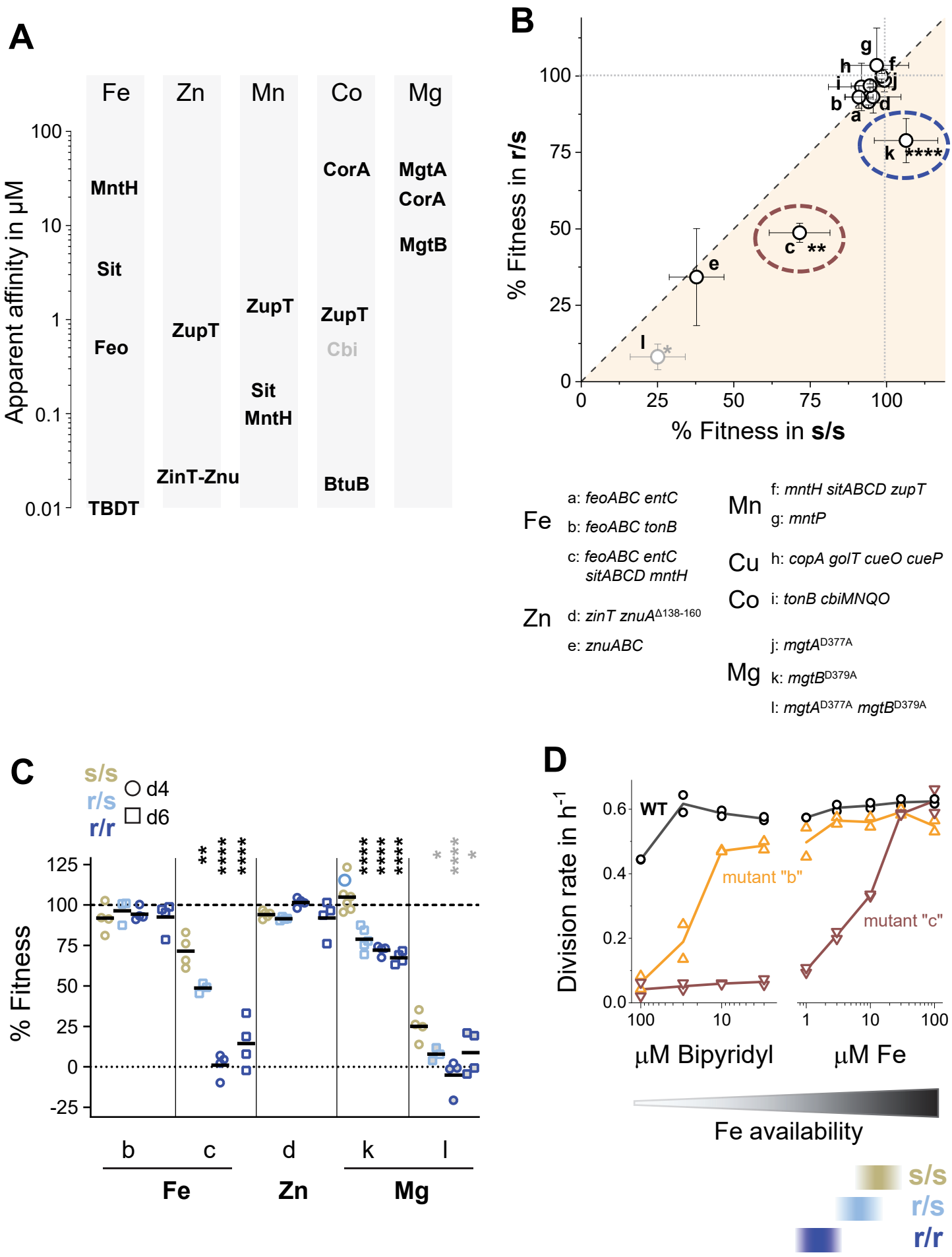
A
Fe
Zn
Mn
Co
Mg
Apparent affinity in µM
100
10
1
0.1
0.01
MntH
Sit
Feo
TBDT
ZupT
ZinT-Znu
ZupT
Sit
MntH
CorA
ZupT
Cbi
BtuB
MgtA
CorA
MgtB
B
% Fitness in r/s
% Fitness in s/s
0
25
50
75
100
a
b
c **
d
e
f
g
h
i
j
k ****
l *
Fe
a: feoABC entC
b: feoABC tonB
c: feoABC entC sitABCD mntH
Zn
d: zinT znuA Δ138-160
e: znuABC
Mn
f: mntH sitABCD zupT
g: mntP
Cu
h: copA golT cueO cueP
Co
i: tonB cbiMNQO
Mg
j: mgtA D377A
k: mgtB D379A
l: mgtA D377A mgtB D379A
C
s/s
r/s
r/r
d4
d6
% Fitness
125
100
75
50
25
0
-25
b
c
d
k
l
Fe
Zn
Mg
D
Division rate in h-1
0.6
0.4
0.2
0.0
WT
mutant "b"
mutant "c"
100
10
1
10
100
µM Bipyridyl
µM Fe
Fe availability
s/s
r/s
r/r

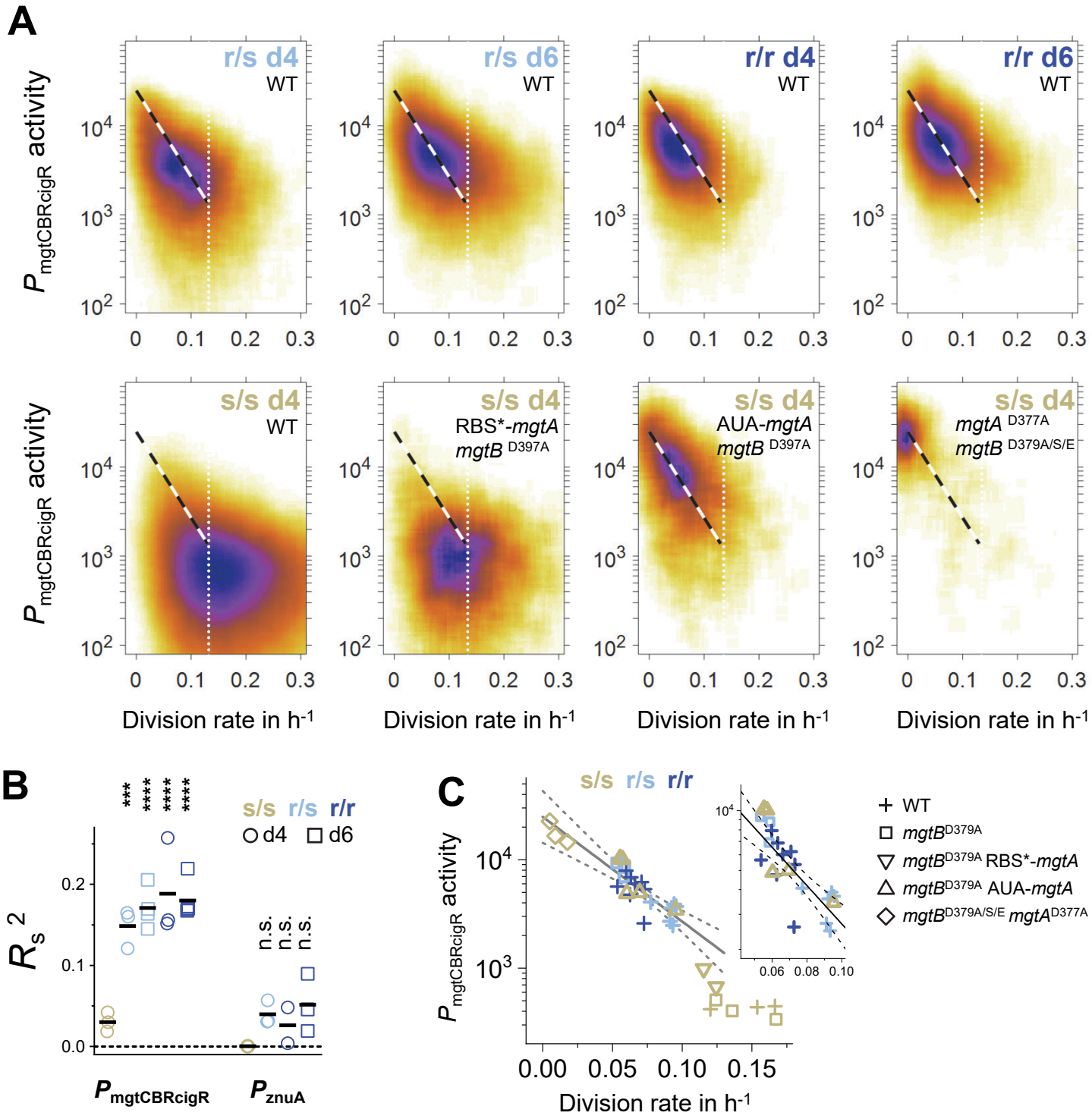
A
r/s d4
WT
r/s d6
WT
r/r d4
WT
r/r d6
WT
s/s d4
WT
s/s d4
RBS*-mgtA
mgtB D397A
s/s d4
AUA-mgtA
mgtB D397A
s/s d4
mgtA D377A
mgtB D379A/S/E
P mgtCBRcigR activity
Division rate in h-1
B
s/s r/s r/r
d4 d6
R s 2
***
****
****
****
n.s.
n.s.
n.s.
P mgtCBRcigR
P znuA
C
s/s r/s r/r
P mgtCBRcigR activity
Division rate in h-1
WT
mgtBD379A
mgtBD379A RBS*-mgtA
mgtBD379A AUA-mgtA
mgtBD379A/S/E mgtAD377A

Supplementary Materials for

Host-resistance factor SLC11A1 restricts *Salmonella* growth through magnesium deprivation

Olivier Cunrath, Dirk Bumann

Correspondence to: dirk.bumann@unibas.ch

This PDF file includes:

Materials and Methods
Supplementary Text
Figs. S1 to S7
Table S1

Materials and Methods

Microbiology and Molecular Biology

Salmonella strains used in this study were based on SME51, a prototrophic *hisG*^{Leu69} derivative of *Salmonella enterica* serovar Typhimurium SL1344 (*1-3*). *Salmonella* strains with gene deletions (preserving a nonapeptide with the first five and last four amino acids, and the stop codon) or point mutations were obtained by two consecutive single-crossovers with positive selection for resistance to kanamycin and negative selection against levan sucrase-mediated sensitivity to sucrose. MgtA abundance was modulated by replacing the wild-type ribosomal binding site gcg**G**aggga with the variant gcg**C**aggga (*4*), or by replacing the wild-type initiation codon AU**G** with AU**A** (*5*).

Reporter strains carried low-copy episomal pSC101-derivatives with constitutive expression of *mCherry* or *mtagbfp2* from the P_{ybaJ} promoter (*6*), and fusions of candidate promoters ($P_{mgtCBRcigR}$, chromosomal coordinates in SL1344 GenBank: FQ312003.1: 3,987,050 - 3,986,453; P_{znuA}, 1,945,050 - 1,944,940) driving expression of *mtagbfp2-ova* coding for a degradable variant (*4*) of the blue fluorescent protein mTagBFP2. Bacteria were grown in Lennox lysogeny broth (LB) or in MES-MM (100 mM MES-KOH pH 5.5, 0.4% glycerol, 15 mM NH_4Cl, 1.5 mM K_2SO_4, 3 mM KH_2PO_4) (*7*) containing 5 mM ascorbate.

Generation of C57BL/6-SLC11A1$^{r/s}$ mice

SLC11A1 was edited using Cas9/CRISP directly in fertilized mouse oocytes. C57BL/6J female mice underwent ovulation induction by i.p. injection of 5 IU equine chorionic gonadotrophin (PMSG; Folligon–InterVet), followed by i.p. injection of 5 IU human chorionic gonadotropin (Pregnyl–Essex Chemie) 48 h later. For zygote recovery, C57BL/6J females were mated with males of the same strain immediately after the administration of human chorionic gonadotropin. All zygotes were collected from oviducts 24 h after the human chorionic gonadotropin injection, and were then freed from any remaining cumulus cells by a 1–2 min treatment of 0.1% hyaluronidase (Sigma-Aldrich) dissolved in M2 medium (Sigma-Aldrich). Mouse embryos were cultured in M16 (Sigma-Aldrich) medium at 37°C and 5% CO2. For micromanipulation, embryos were transferred into M2 medium. All microinjections were performed using a microinjection system comprised of an inverted microscope equipped with Nomarski optics (Nikon), a set of micromanipulators (Narashige), and a FemtoJet microinjection unit (Eppendorf). Injection solution containing 300 ng/ul in-vitro transcribed sgRNA$^{(F+E)}$ (*8*) targeting the sequence atcagtacaccgtcccacagcgg, 20 ng/ul ssDNA homologous recombination template aagctggccaagctatttgggttcctgactccccagatctgggtcaggctgattgatctgccctacttggtttcagcatcccattatggggaggagttctgatcaccattgtggacaccttcttcttcctcttcttggataactatggtgagagaaagccccctcatcttgggggataa (IDT), 50 ng/µl Cas9 protein (Toolgenl) was microinjected into the male pronuclei of fertilized mouse oocytes until 20-30% distension of the organelle was observed. Embryos that survived the microinjection were transferred on the same day into the oviducts of 8 to 16 week-old pseudo-pregnant Crl:CD1(ICR) females (0.5 days after coitus) that had been mated with sterile genetically vasectomized males (*9*) half a day before. Pregnant females were allowed to deliver and raise their pups until weaning age.

A female mouse carrying one *SLC11A1*^{r} (G169) allele was identified using PCR of genomic DNA with primers oOPC-048, aagctatttgggttcctgactccc; oOPC-049, cccaagatgaggggctttctctc, and oOPC-525, tggtgatcagaactcctccccataat. This yielded two fragments of 160 and 80 bp, instead of only a single fragment with 160 bp for parental C57BL/6J mice

carrying two *SLC11A1*^{s} (D169) alleles. We used http://crispr.mit.edu/ to predict 49 potential off-target sites with scores between 0.2 and 1.4 (the on-target score was 82). We sequenced the top two off-targets (chr6:146,977,326; chr11:96,132,107) and two other off-targets, that were the only ones associated with exons (chr9:96,844,606, USCS gene NM_145134; chr9:106,366,025, NM_021567) and found no mutation in any of them compared to the parental C57BL/6J genome. The founder mouse was mated with C57BL/6J males. Offspring was characterized with the same PCR and an additional PCR with primers oOPC-048, oOPC-49, and oOPC-524, atcagtacaccgtcccacagc, which yielded two fragments (80, 160 bp) if at least one *SLC11A1*^{s} allele was present, but only a single 160 bp fragment for *SLC11A1*$^{r/r}$ homozygotes.

Mouse Infections and Tissue Collection

All animal experiments were approved (license 2239, Kantonales Veterinäramt Basel) and performed according to local guidelines (Tierschutz-Verordnung, Basel) and the Swiss animal protection law (Tierschutz-Gesetz). Sex-matched 10 to16 week-old littermates were infected by tail vein injection of *Salmonella* strain mixtures containing 1,000 to 3,000 CFU in 100 µl PBS. The inoculum size was determined by plating for each infection. Mice were scored daily for disease signs (unprovoked behavior: normal – 0, minor changes – 1, less mobile and isolated – 2, restless and very still – 3; provoked behavior: responsive & alert – 0, unresponsive & not alert – 3; physical appearance: normal – 0, lack of grooming – 1, piloerection – 2, hunched up – 3, eyes half closed – 4; clinical signs: normal respiratory rate – 0, slight changes – 1, decreased rate and abdominal breathing – 2, marked abdominal breathing & cyanosis – 3; hydration status: normal – 0, dehydrated – 5; strength (grip test): grab and pull – 0, grab but no pull – 2, neither grab nor pull – 4; surface temperature was not indicative of progressive disease; maximum combined score 22). Four or six days post-infection, the mice were euthanized with carbon dioxide and the spleen was prepared. *Salmonella* load was determined by plating and flow cytometry. Fitness was calculated as $\log_2$(FI) with FI corresponding to the fold increase starting from the initial spleen colonization (around 20% of the total inoculum (*10*)) to the final spleen load. The relative fitness value of co-administered wild-type *Salmonella* was set to 100%. We also determined the more commonly used read-out "competitive index" (CI) by dividing the output ratio (mutant/wild-type) by the inoculum ratio (mutant/wild-type) (fig. S3). In contrast to relative fitness, CI values increasingly diverge from 1 with ongoing division. Because *Salmonella* divided more slowly in (r/s) mice compared to (s/s) mice (Fig. 1F), CI values underestimated the mutant phenotypes in (r/s) mice.

We estimated sample size by a sequential statistical design. We first infected two to three mice based on effect sizes and variation observed in our previous studies (*11*), and used the results to estimate group sizes for obtaining statistical significance with sufficient power. The experiments were neither randomize nor blind. However, flow cytometry analysis was carried out using an automated unbiased approach (see Flow Cytometry section).

Flow Cytometry

The spleen was homogenized in ice-cold PBS containing 0.2% Triton X-100. All samples were kept on ice until and during analysis. Large host cell fragments were removed by centrifugation at 500xg for 5 min. Relevant spectral parameters were recorded in a FACS Fortessa II equipped with 405 nm, 488 nm and 561 nm lasers (Becton Dickinson), using thresholds on SSC and FSC to exclude electronic noise. We used the following channels: mTagBFP2, excitation 405 nm, emission 460-480 nm ("blue"); GFP and green TIMER^{bac}

component, excitation 488 nm, emission 502-525 nm ("green"); mCherry and orange TIMER^{bac} component, excitation 561 nm, emission 595-664 nm ("orange"); yellow autofluorescence channels, excitation 445 nm, emission 573-613 nm; or excitation 488 nm, emission channels 533-551 nm, 573-613 nm. NeonGreen- or YPet-expressing *Salmonella* cells were purified from infected spleen homogenates using an Aria IIIu cell sorter (BD Biosciences) using excitation 488 nm and emission channels 499-529 nm (NeonGreen) or 533-551 nm (YPet), and 573-613 nm for separating host autofluorescence, in presence of 170 mg l^{-1} chloramphenicol to prevent *de-novo* protein biosynthesis. Data were processed with FlowJo, FCS Express, and MATLAB. TIMER^{bac} fluorescence log color ratios (green/orange) were converted into *Salmonella* division rates based on a previously established calibration data (*3*).

Proteomics

We purified between $1.5x10^6$ and $9x10^6$ *Salmonella* cells from individual *SLC11A1*$^{s/s}$, *SLC11A1*$^{r/s}$, and *SLC11A1*$^{r/r}$ mice (three to five mice for each genotype). We processed the sorted *Salmonella* with the sample preparation kit from PreOmics (PreOmics GmbH, Germany) according to the protocol version 2.2. The cell pellets were lysed in 50 µl of the provided lysis buffer and heated for 5 min at 95 °C. The samples were sonicated with a Bioruptor (Diagenode) applying the standard 10 min method (30 s on, 30 s off, 10 cycles). The protein concentration was determined by BCA assay (Thermo-Pierce, 23252). A maximum of 100 µg protein was digested at 37 °C for four hours. After clean-up according to the manufacturer's procedure, the peptides were dried in a vacuum centrifuge and frozen at -20 °C until further use.

Data independent analysis (DIA) was performed using a previously described method on an high mass-accuracy and resolution mass spectrometer (Q-Exactive HF coupled online to an Easy-nLC-system, Thermo-Fisher Scientific) (*12*). Peptide separation was performed over 90 min. The HRM DIA method contained an MS1 scan (target setting: 5e6 ions, maximum accumulation time: 100 ms, scan range: 400-1220 m/z, resolution: 120,000 FWHM) followed by acquisition of 38 DIA windows (target setting: 3e6 ions, maximum accumulation time: auto, resolution: 30,000 FWHM). Stepped collision energy was 22.5%, 25%, 27.5%. Spectra were recorded in profile mode.

Data files were converted to htrms file format using HTRMS Converter (Biognosys AG, Switzerland). Converted files were imported into Spectronaut 11 (Biognosys AG, Switzerland) using default parameters with the following exceptions for the quantification settings: no cross run normalization and only proteotypic peptides allowed. An in-house *Salmonella enterica* serovar Typhimurium SL1344 spectral library was generated from *Salmonella* grown under different standard media conditions and from *Salmonella* purified from mouse spleen. This spectral library was merged with an in-house generated mouse spectral library. Peptide and protein identification was performed allowing a q-value of 0.01. Protein abundance was calculated from the protein group quantity calculation (PG quantity) as provided by the software and the protein's molecular weight. Samples were normalized assuming a total protein content of 190 fg per cell.

Confocal microscopy

2-3mm thick spleen sections from mice that received 20 nanomole of the cathepsin probe iABP (*13*) (Vergent Bioscience) i.v. 1 h before harvesting, were fixed with fresh 4% paraformaldehyde at 4°C for 4 h, followed by incubating in increasing sucrose concentrations from 10%-40% at 4°C. After overnight incubation in 40% sucrose, tissue was rapidly frozen in

embedding media (Tissue-Tek® O.C.T; Sakura), and then stored at -80°C. 10-14 µm thick cryosections were cut, put on coated glass cover slips (Thermo Scientific), and dried in a desiccator. Sections were mounted in fluorescence mounting medium (Dako), and examined with a Zeiss LSM 880 confocal microscope using glycerol 40X and 63X objectives.

Statistics

Statistical tests were performed with GraphPad Prism 8.0.2 as indicated in the figure legends.

Supplementary Text

Genotypes of *Salmonella* iron-transport mutants:

"a", *feoABC entC*: lacks the high-affinity transporter for Fe^{2+} FeoABC and is defective for biosynthesis of *Salmonella* siderophores for high-affinity uptake of Fe^{3+}

"b", *feoABC tonB*: lacks the high-affinity transporter for Fe^{2+} FeoABC and TonB required for high-affinity uptake of ferri-siderophores (*14*), including mammalian ferri-2,5-dihydroxybenzoic acid (gentisic acid) (*15, 16*)

"c", *feoABC entC sitABCD mntH*: lacks the high-affinity transporter for Fe^{2+} FeoABC and moderate-affinity transporters for Fe^{2+} SitABCD and MntH (which also transport Mn^{2+} with high affinity), and is defective for biosynthesis of *Salmonella* siderophores for high-affinity uptake of Fe^{3+}

Zinc-transport mutants

"d", *zinT znuA*$^{\Delta 138\text{-}160}$: lacks the auxiliary periplasmic Zn^{2+}-binding protein ZinT and carries a variant of the other periplasmic Zn^{2+}-binding protein ZnuA with reduced loading capacity for Zn^{2+} to the membrane transporter ZnuBC (*17, 18*)

"e", *znuABC*: lacks the high-affinity Zn^{2+} ABC transporter

Manganese-transport mutants

"f" *mntH sitABCD zupT*: lacks the high-affinity transporters for Mn^{2+} SitABCD and MntH (which also transport Fe^{2+} with moderate affinity) and the moderate-affinity Mn^{2+} transporter ZupT (which also transports Zn^{2+} and Co^{2+})

g: *mntP*: lacks the Mn^{2+} exporter MntP

Copper-transport mutant

h: *copA golT cueO cueP*: lacks export and binding proteins involved in copper resistance

Cobalt-transport mutant

i: *tonB cbiMNQO*: lacks TonB-dependent vitamin B12 uptake through BtuB and the high-affinity Co^{2+} transporter CbiMNQO

Magnesium-transport mutants

We inactivated MgtA and MgtB by mutating crucial aspartate residues (*19*) instead of full gene deletions, in order to minimize polar effects on their complex genetic loci with multiple promoters, protein coding genes, non-coding RNAs, and extensive post-transcriptional regulation (*19-30*).

j: *mgtA*^{D377A}: inactive moderate-affinity transporter MgtA

k: *mgtB*^{D379A}: inactive moderate-affinity transporter MgtB

l: *mgtA*^{D377A} *mgtB*^{D379A}: both MgtA and MgtB are inactive

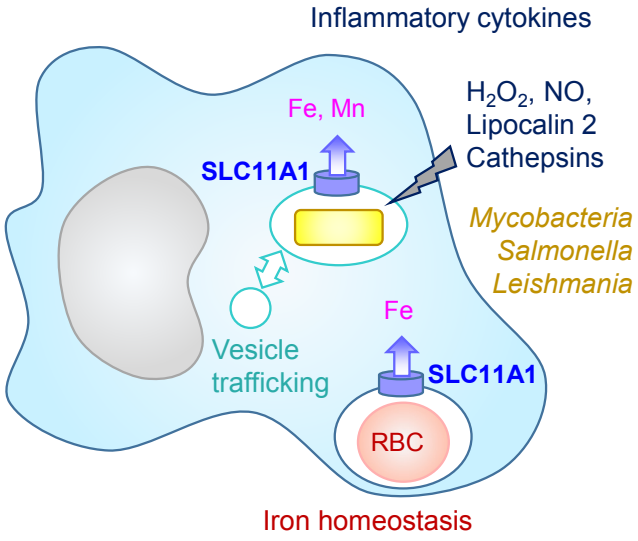

Fig. S1. Pleiotropic impact of SLC11A1 during infection with diverse intracellular pathogens. SLC11A1 transports the divalent metal cations Fe^{2+}, Mn^{2+} out of phagosomes (*31-33*), and may deprive vacuolar pathogens of these essential micronutrients (*34-36*). In addition, SLC11A1 has pleiotropic effects on phagosome maturation (*37-39*); pro-inflammatory cytokines (*34, 40*) and activation of innate lymphocytes (*41*); generation of antimicrobial effector molecules such as nitric oxide (NO) (*34, 42, 43*), reactive oxygen species such as hydrogen peroxide (H_2O_2) (*36, 43*), and lipocalin 2 (*36*). SLC11A1 contributes to iron homeostasis by facilitating recycling of iron from aged red blood cells (RBC) (*44-47*).

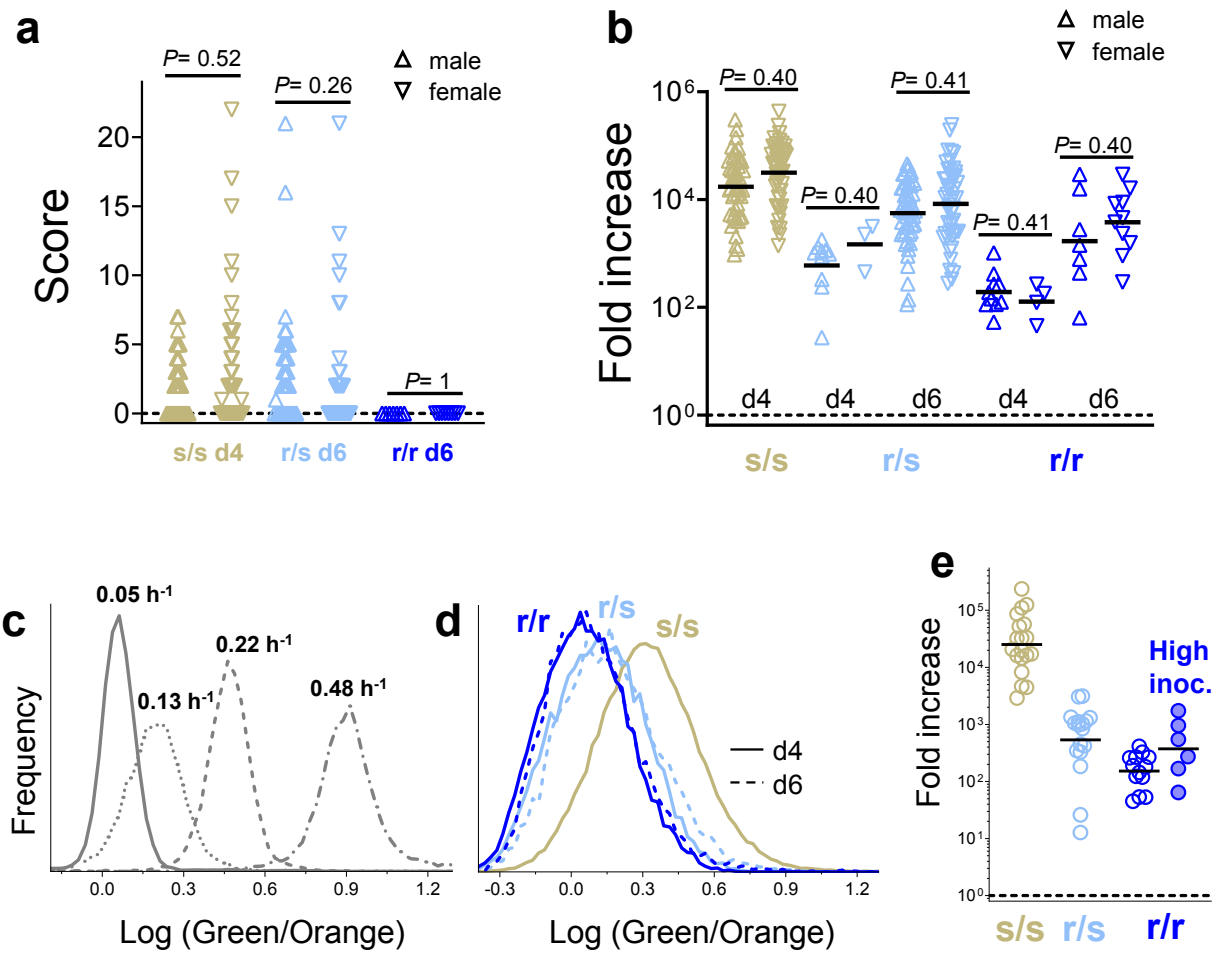

Fig. S2. Responses to *Salmonella* infection in different mouse genotypes. (**a**) Scores for disease symptoms in male and female mice (d4, day 4; d6, day 6). Each symbol represents a single mouse. Statistical differences between sexes were tested according to Kolmogorov-Smirnov with Holm-Šídák correction for multiple testing. (**b**) Growth of *Salmonella* in spleen of male and female mice. Statistical differences between sexes were tested with One-way ANOVA of log-transformed values with Holm-Šídák correction. (**c**) Fluorescence properties of *Salmonella* expressing the division-rate reporter TIMER^{bac} when growing at defined rates *in vitro* (new representation of data reported in (*3*)). (**d**) TIMER^{bac}-*Salmonella* fluorescence properties in spleen. Data for five to ten mice were pooled. (**e**) *Salmonella* spleen growth until day 4 post-infection after infection with about 1,000 CFU or about 50.000 CFU (High inoc.).

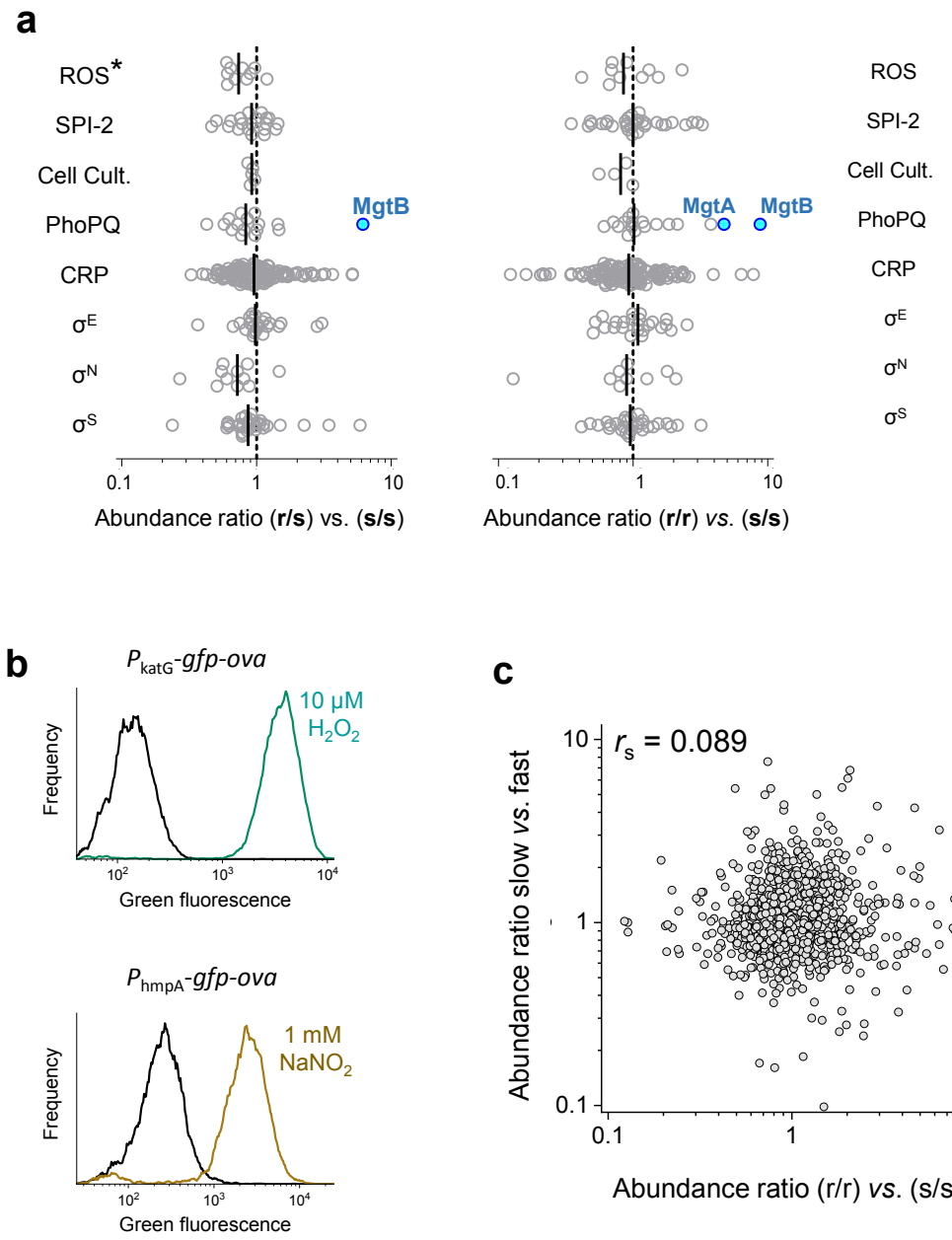

Fig. S3. Proteome analysis of *Salmonella* purified from different mouse genotypes. (**a**) Comparison of *Salmonella* protein abundances between *SLC11A1*$^{s/s}$ and *SLC11A1*$^{r/s}$ or *SLC11A1*$^{r/r}$ mice for proteins associated with defense against reactive oxygen species (ROS), *Salmonella* pathogenicity island 2 (SPI-2), previous findings for SLC11A1-dependent proteins in cell culture infections (Cell Cult.), the PhoPQ regulon, the cAMP receptor protein CRP, or

various sigma factors of the RNA polymerase. Each circle represents one protein. The magnesium transporters MgtA and MgtB are part of the PhoPQ regulon and get additionally upregulated at low Mg^{2+} availability (*, $P< 0.05$; One-sample Wilcoxon signed rank test with Holm-Šídák correction for multiple testing). Carbon and nitrogen availability seemed to be similar based on the expression of target genes of CRP, σ^N, and σ^S. The same was true for extracytoplasmic stress based on σ^E targets. In addition to data shown in this figure, nitric oxide denitrosylase HmpA, a signature protein of Salmonella exposure to reactive nitrogen species (41) (abundance ratio (r/s) vs. (s/s), 1.2 ± 0.4; (r/r) vs. (s/s), 0.41 ± 0.2) and phosphate starvation markers PhoB (abundance ratios, 1.0 ± 0.3, 0.8 ± 0.3) and PstS (1.1 ± 0.4, 1.4 ± 0.4) were of comparable abundance. (**b**) Green fluorescence of *Salmonella* carrying promoter fusions P_{katG}-*gfp-ova* or P_{hmpA}-*gfp-ova* under *in vitro* control conditions without oxidative and nitrosative stress (black), or after exposure to hydrogen peroxide for 30 min, or nitrite at pH 5.5 for 60 min, respectively. (**c**) Comparison of protein abundance ratios in (r/s) *vs*. (s/s) mice, to protein ration in fast- *vs*. slow- -growing subsets in BALB/c (s/s) mice (data from (*3*); r_s, Spearman's rank correlation coefficient).

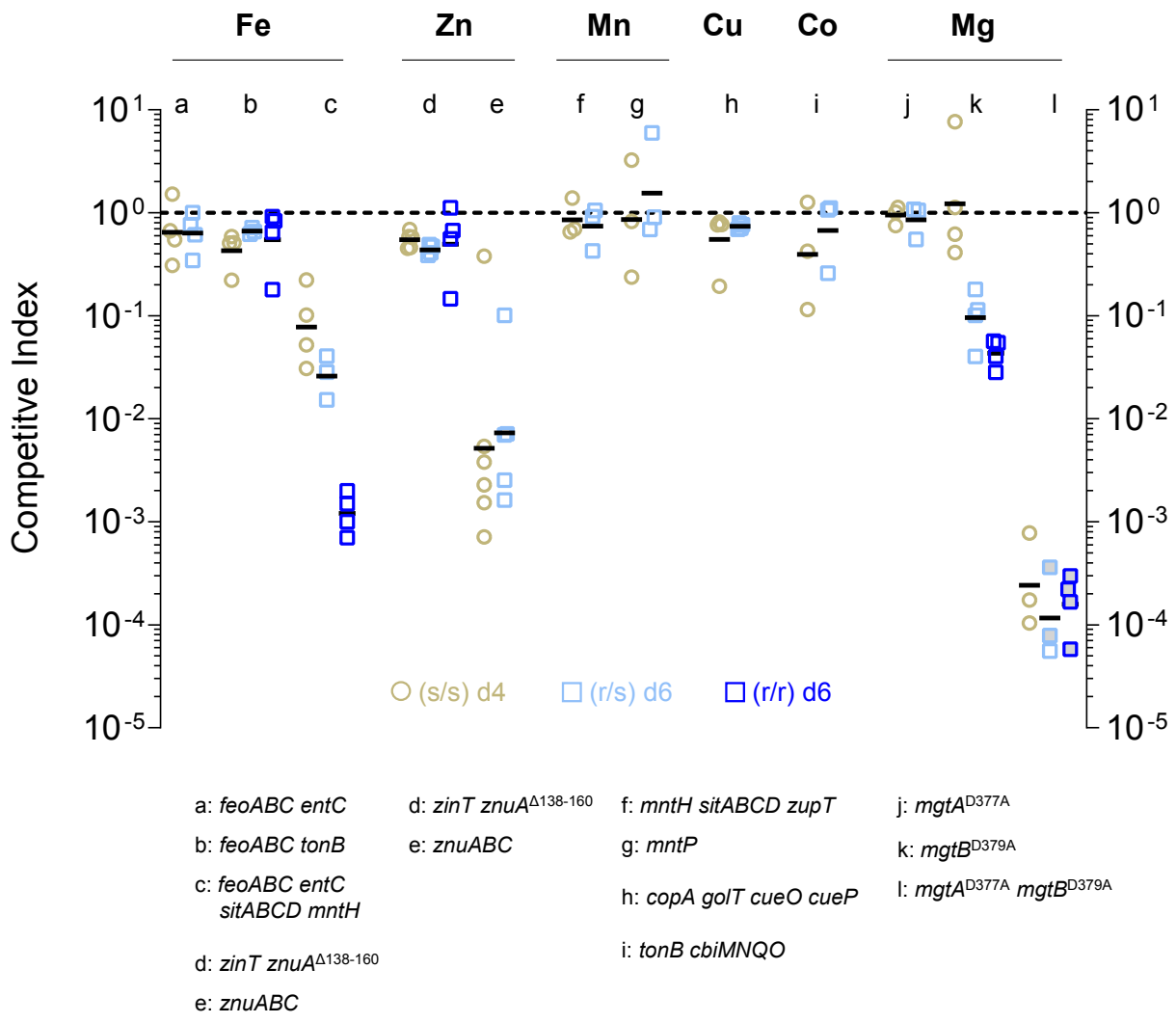

Fig. S4. Competitive indices of *Salmonella* mutants in *SLC11A1*$^{s/s}$ (s/s), *SLC11A1*$^{r/s}$ (r/s), or *SLC11A1*$^{s/s}$ (r/r) mice. Mice were infected with mixtures of *Salmonella* wild-type and *Salmonella* mutants, and the competitive index for each mutant was calculated by dividing the output ratio (mutant/wildtype) by the input (mutant/wildtype). The dashed line at a value of 10^0 represents wild-type fitness. Each circle represents a single mouse, the lines show the geometric means. Only mutants "b", "c", "d", "k", and "l" were tested in (r/r) mice. Data below the limit of detection (LOD) were substituted by LOD/√2 and are shown in grey. In contrast to relative fitness data shown in Fig. 3B,C, competitive indices increasingly diverge from 1 with ongoing divisions. Because *Salmonella* divided more slowly in (r/s) and (r/r) mice compared to (s/s) mice, CI values underestimated the mutant phenotypes in (r/s) and (r/r) mice relative to (s/s) mice.

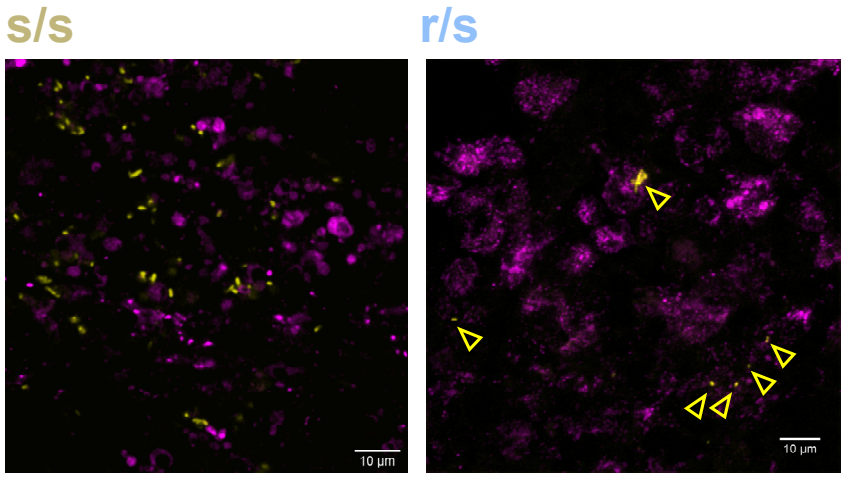

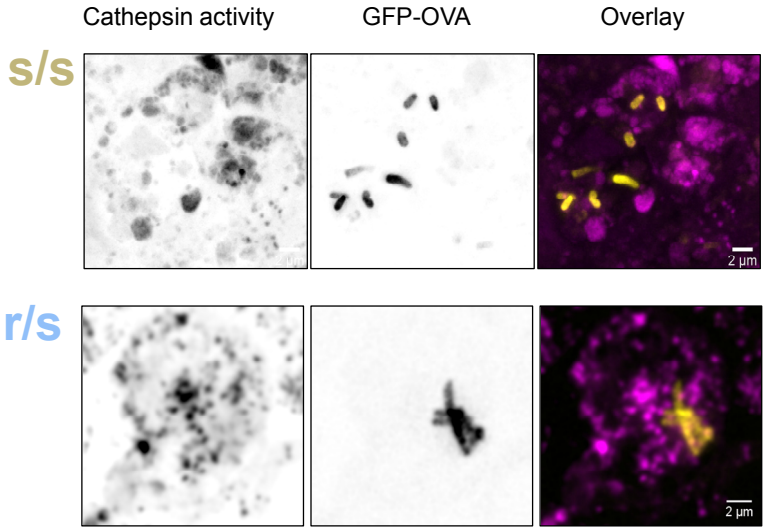

Fig. S5. Localization of cathepsin activities and *Salmonella* cells in spleen. Cathepsin activites (magenta, quenched-activity based probe iABP) and GFP/YPet fluorescence of *Salmonella* cells (yellow) in spleens of *SLC11A1*$^{s/s}$ (s/s) and *SLC11A1*$^{r/s}$ (r/s) mice. The upper panels show confocal micrographs of spleen cryosections. The lower panels show for each mouse genotype one infected cell with high cathepsin activities but no detectable co-localization, at higher magnification. Similar images were obtained for sections from three independently infected *SLC11A1*$^{r/s}$ mice. Infected control mice with no iABP injection showed only faint background signals.

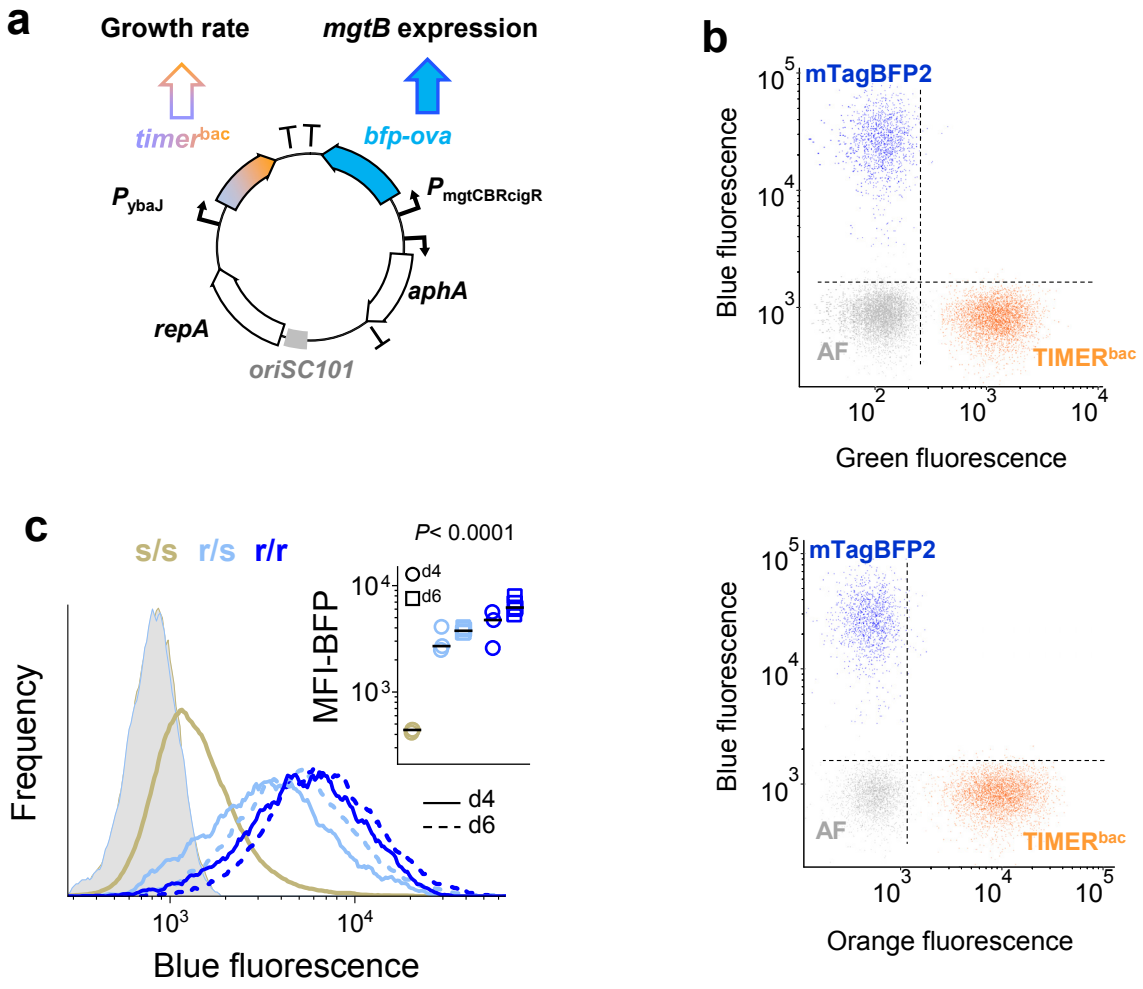

Fig. S6. Measurement of correlations between *Salmonella* replication and transporter expression. (**a**) Map of dual reporter plasmid (*timer*^{bac} codes for the growth rate reporter TIMER^{bac} (*3*); *bfp-ova* codes for a fusion of the blue fluorescent protein mTagBFP2 with an ovalbumin peptide that increases proteolysis of fluorescent proteins (*4*) for reporting current promoter activities with minimal contributions from previous expression; T, terminator; *aphA* confers resistance to kanamycin; *repA* codes for replicase recognizing the origin of replication, *oriSC101*). (**b**) Flow cytometry of *Salmonella* strains expressing mTagBFP2, TIMER^{bac}, or neither of the two fluorescent proteins (autofluorescence, AF) in spleen homogenates. The dashed lines represent upper limits of autofluorescence. mTagBFP2 and TIMER^{bac} have orthogonal fluorescence colors with no bleed-through in blue / green fluorescence channels

(upper panel) and blue / orange fluorescence channels (lower panel). (**c**) Blue fluorescence of *Salmonella* carrying the dual reporter plasmid shown in (a) in mice with different *SLC11A1* genotypes. The shaded histograms represent autofluorescence of *Salmonella* with no BFP expression. Histograms represent pooled data for three to five mice. The inset shows median BFP fluorescence intensities corrected for blue autofluorescence (MFI-BFP) with each symbol representing a single mouse (*P*-value for One-way ANOVA with test for linear trend). *Salmonella* stably maintained the plasmid during infection without detectable fitness impairment (< 1% plasmid loss after six days based on fluorescence of colonies grown *ex vivo* on non-selective medium). $P_{mgtCBRcigR}$ activity was 7.2 to 15 fold higher in (r/s) and (r/r) mice compared to (s/s) mice, consistent with 6.2 ± 2.7 and 8.7 ± 2.3 fold higher abundance of the MgtB protein in (r/s) and (r/r) mice, respectively (Fig. 2A).

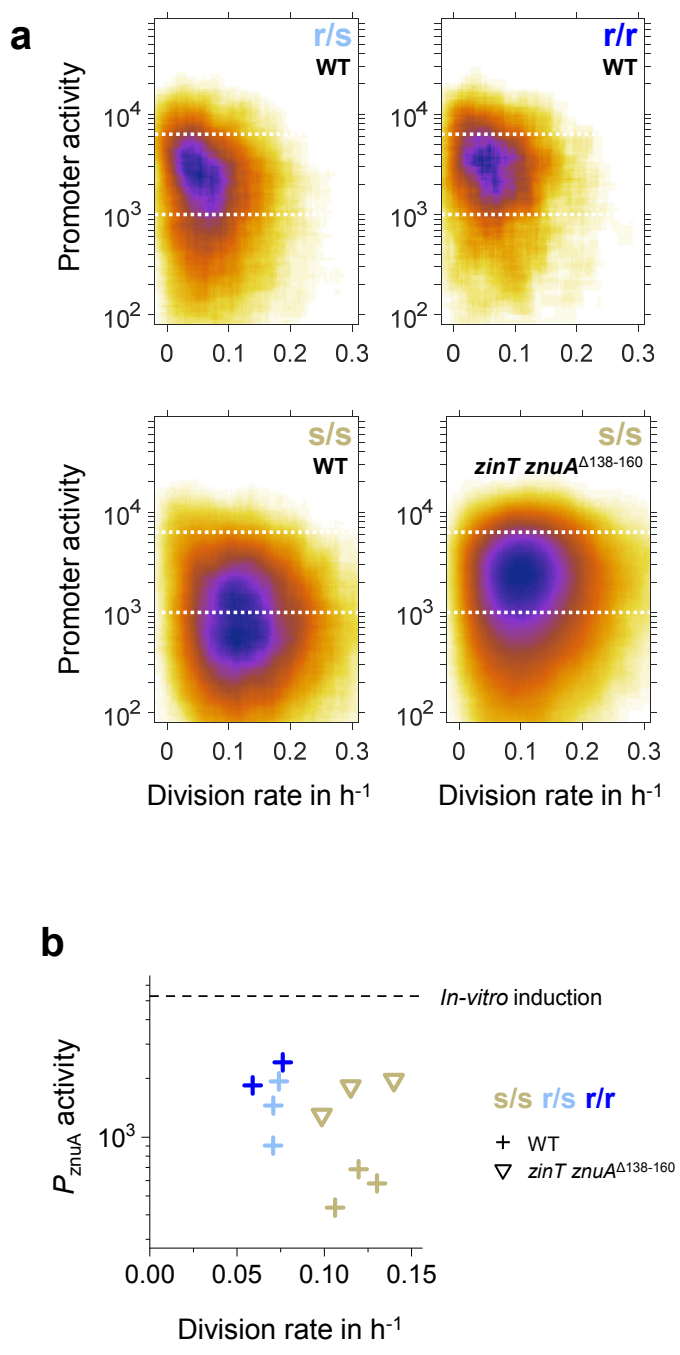

Fig. S7. Relation between *Salmonella* replication and expression of the zinc transporter gene *znuA*. (**a**) *Salmonella* division rates based on TIMER^{bac} emission color, and P_{ZnuA} activities at day 4 post-infection. *znuA* encodes the crucial periplasmic Zn^{2+}-binding protein ZnuA (*18*), which is strongly induced by zinc starvation (*48*). The plots represent pooled data from two to

three mice. The doted white lines represent the range that contains the majority of P_{znuA} activities in (r/s) and (r/r) mice. P_{znuA} activity was 2.5 ± 1.1 fold higher in (r/s) mice and 3.8 ± 1.1 fold higher in (r/r) mice compared to (s/s) mice, consistent with higher abundance of the ZnuA protein in (r/s) and (r/r) mice (2.4 ± 0.6 fold, 2.8 ± 0.5 fold; Fig. 2A). (**b**) Median division rates and P_{znuA} activities for *Salmonella* strain/mouse genotypes shown in (a). Each symbol represents a single mouse. Symbol shapes represent *Salmonella* genotype and symbol colors represent mouse genotype. *In-vitro* induction levels in lysogeny broth containing 100 μM EDTA are shown for comparison. The zinc-uptake mutant *Salmonella zinT znuA*$^{\Delta 138\text{-}160}$ (mutant "d") had as high *znuA* expression levels in (s/s) mice (3.0 ± 0.9 fold), as wild-type *Salmonella* in (r/s) and (r/r) mice, but nevertheless maintained high division rates consistent with the only slight attenuation of this mutant (Fig. 3B,C) (*17, 18*).

Transporter	References	Fe	Zn	Mn	Co	Mg	comment
TBDT	(*49*)	0.5 nM					ferri-siderophore
FeoABC	(*50*)	0.5 μM					
SitABCD	(*51*)	3 μM		0.1 μM			
MntH	(*52*)	25-50 μM		0.1 μM			at pH 5.5
ZinT-ZnuABC	(*53*)		< 20 nM				
ZupT	(*54*)		0.71 μM	1.16 μM	0.91 μM		
BtuB	(*55*)				16 nM		cob(I)alamin
CorA	(*56, 57*)				30 μM	15 μM	
MgtA	(*57*)					29 μM	
MgtB	(*57*)					6 μM	

Table S1. Apparent metal affinities of divalent cation transporters (as shown in Fig. 3A).